Aerodynamic Characteristics of a Flexible Membrane Wing

S. Greenhalgh*
Naval Air Development Center, Warminster, Pennsylvania
and
H. C. Curtiss Jr.†
Princeton University, Princeton, New Jersey

The results of experimental studies of the aerodynamic characteristics of single-surface membrane wings constructed of inextensible flexible material are described and compared with theory. The experiments included measurement of the lift and drag characteristics of semispan wing models of three different planforms (triangular, parabolic, and elliptical). The wing surfaces were constructed of 2- and 4-mil stainless steel shim stock attached to a streamline leading-edge spar. This very thin metal membrane is flexible and adjusts its shape in response to the airflow over the wing surface. The experimental apparatus permitted variation of the camber and twist distribution of the wing. A unique method of describing the geometry of the wing is presented and used to correlate the experimental results and to compare experiment with theory. The experimental results agree well with lifting line theory below stall using the method presented for determining the geometric shape of the wing. The wing with the parabolic planform exhibited the best aerodynamic characteristics compared to the triangular and elliptical planforms. The maximum lift coefficients and lift-to-drag ratios measured are comparable to conventional rigid wings. Various dynamic phenomena encountered during the experiments are described.

Nomenclature

b = wing span, in. or cm
c_0 = membrane root chord, in. or cm
c_e = chord of leading-edge spar
C_L = wing lift coefficient
c_r = wing root chord $c_r = c_e + c_0$
$c(y)$ = local membrane chord, in. or cm
L = virtual apex location from root of wing, positive outboard, in. or cm
m = camber ratio
Re = Reynolds number based on root chord
x = chordwise station on wing measured from leading edge of membrane, in. or cm
x^* = chordwise location at wing root corresponding to spanwise location
x_m = chordwise location of maximum camber point
XL = excess length $XL = 100 \times [(\ell + c_e - c_r)/c_r]$
y = spanwise location on wing, in. or cm
z = height to camber line at root of wing, in. or cm
$\mathcal{R}$ = wing aspect ratio
ϕ_A = aerodynamic twist of wing, positive for wash-in, rad
ϕ_G = geometric twist of wing, positive for wash-in, rad
ℓ = membrane length at wing root, in. or cm

Subscripts and Superscripts

$(\bar{\ })$ = quantity nondimensionalized by membrane root chord
$(\hat{\ })$ = quantity nondimensionalized by semispan

Introduction

SINGLE-SURFACE flexible lifting wings have many possible applications owing to low cost and simplicity of construction, provided that their aerodynamic characteristics are desirable and that their dynamic behavior can be satisfactorily understood and quantified. This investigation of membrane wings is a continuation of earlier two-dimensional studies conducted on inextensible flexible membrane airfoils.[1] While the two-dimensional or sectional characteristics of membrane airfoils have been the subject of many investigations (e.g., Refs. 2 and 3), there is little experimental data on the aerodynamic and dynamic characteristics of single-surface wings in general and no experimental data or theory for wings formed from an inextensible flexible material.

The investigation of the characteristics of single-surface wings has been the subject of a number of previous studies.[4-10] Curry[4] was perhaps the first to conduct investigations of the aerodynamics of such wings for application to sail aerodynamics.

In his book, Curry presents wind tunnel data collected during 1923-1924 on rigid sheet metal airfoils and wings of various shapes, cambers, and twist. There is a description of visual observations of the flowfield using down feathers as a probe. Tanner[5] and Marchaj[6] of the University of Southampton have considered both experimental and theoretical aspects of sail design. They achieved limited success in their experimental studies primarily because of the difficulty of performing controlled wind tunnel tests on scale models with fabric surfaces.

Other studies include Milgram's[7] theory for sail design optimization using lifting line theory and Jackson's[8] vortex lattice/finite element approach to the coupled aerodynamic/structural problem of a single-surface flexible elastic lifting membrane.

Ormiston[9] undertook an extensive experimental and theoretical study of the Princeton Sailwing concept (a double-surface wing) in the late 1960s and has recently conducted some studies on four full-scale ultralight gliders at NASA Ames. The research was directed toward the investigation of the performance and longitudinal stability of ultralight vehicles.

The recent work of Kroo[10] involved analytical studies as well as wind tunnel experiments on scale-model hang gliders. The objective of this study was to promote understanding of the overall problem of hang glider performance.

Presented as Paper 84-2168 at the AIAA Second Applied Aerodynamics Conference, Seattle, WA, Aug. 21-23, 1984; received Aug. 23, 1984; revision received April 1, 1985.

*Aerospace Engineer. Member AIAA.
†Professor, Department of Mechanical and Aerospace Engineering. Member AIAA.

It is clear that it is difficult to obtain solutions to the complete aeroelastic equations describing the behavior of a three-dimensional elastic flexible lifting surface. It is also difficult to provide precise control of experiments on single-surface wings constructed of elastic material or fabric. Therefore, it was considered that it would be highly desirable to conduct experiments on a single-surface wing made of material that is inelastic yet flexible. An understanding of this limiting case would be useful in itself and would also offer the possibility of providing a reference point for the more complex case of an elastic membrane.

By constructing the wing surface of an essentially inextensible but still flexible material, the structural aspects of the problem are not present. As a result, a wind tunnel model with precise controllable features that can produce repeatable data is obtained.

Stainless steel shim stock 0.002/0.004 in. (0.05/0.10 mm) thick was selected as the material for the wing surface. The leading edge of the wing surface was attached to a leading-edge spar. One other point, the root trailing edge, was fixed to the reflection plane. The shape of the wing surface was determined by the airflow over the wing and two adjustments: one that precisely locates the chordwise position of the root trailing edge; and the second, at the wing tip, which controls the wing twist distribution as shown in Fig. 1. The location of the wing root trailing edge is characterized by a parameter referred to as the excess length, which is defined as the difference between the membrane length at the root plus the leading-edge spar chord and the root chord, nondimensionalized by the root chord expressed in percent. The camber ratio at the root is approximately related to the excess length by $m \approx 0.061\sqrt{XL}$ (Ref. 1).

The effect of wing tip adjustment is described in terms of a point referred to as the virtual apex. Figure 2 shows the assumed wing surface geometry and the definition of the virtual apex. Since the membrane is inelastic and did not wrinkle under the majority of test conditions, the surface of the wing must be a developable surface or part of an imaginary cone. The virtual apex is the apex of that cone, and the cross section of the cone is determined by the shape of the camber line at the wing root. Since the spar constrains the leading edge of the membrane to be a straight line, the virtual apex must lie on the leading edge or its extension. The location of the virtual apex is expressed in semispans, measured from the root of the wing. Thus, a positive value of 1 corresponds to the apex at the wing tip, and values larger than 1 are outboard of the tip. A negative value corresponds to a location inboard of the root as shown below. The geometric shape of the wing surface is completely specified by the excess length, the virtual apex location, and the shape of the camber line at the root of the wing. The shape of the camber line is determined by the airflow over the wing.

The wind tunnel test results are presented followed by a comparison between theory and experiment. Experimental data were obtained for three wing planforms and a variety of root and tip adjustments. Some qualitative observations on the unsteady behavior of the wings at various test conditions are also included.

Experimental Results

The experiments were conducted using semispan models mounted on a reflection plane in the Princeton University 4-ft (1.22-m) × 5-ft (1.52-m) wind tunnel. The model and wind tunnel details are presented in Table 1 and in Figs. 1 and 3. The triangular wing results presented are for the 0.002-in. (0.05-mm) surface at a Reynolds number based on a root chord of 7×10^5. Except as noted, the parabolic wing results are presented for the 0.004-in. (0.10-mm) surface at a Reynolds number of 5×10^5. Elliptical wing results are for the 0.004-in. (0.10-mm) surface at a Reynolds number of 5×10^5.

Figures 4-8 show measured variations in lift coefficient with angle of attack as a function of virtual apex location for different values of excess length and wing planform. It can be seen that virtual apex location primarily determines the angle of attack of the wing for zero lift. There is a commensurate shift in the angle of attack for maximum lift coefficient with little change in the value of the maximum lift coefficient. It may be noted that the elliptical wing exhibits a lower lift-curve slope than would be expected based on the aspect ratio (Table 1). The reason for this decrease appears to be largely that, because of the highly curved trailing edge, the air pressure acting on the aft portion of the surface deflected the surface upward with increasing angle of attack. This distortion was not observed on the parabolic planform. Figure 9 shows the lift-to-drag ratio as a function of angle of attack for the parabolic planform wing, showing that the primary effect of virtual apex location is to shift the maximum lift-to-drag ratio to a larger angle of attack. Figure 10 shows the effect of varying the excess length at a fixed apex location. The primary effect of increasing excess length is to increase the maximum lift coefficient as would be expected due to an increase in camber.[1] It is interesting to note,

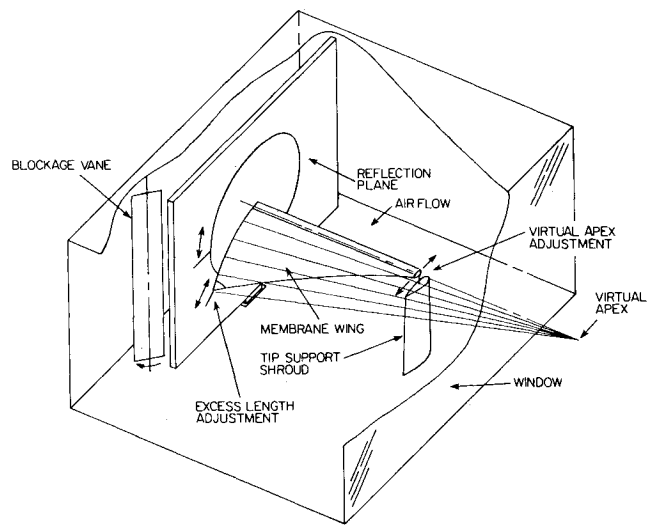

Fig. 1 Experimental setup.

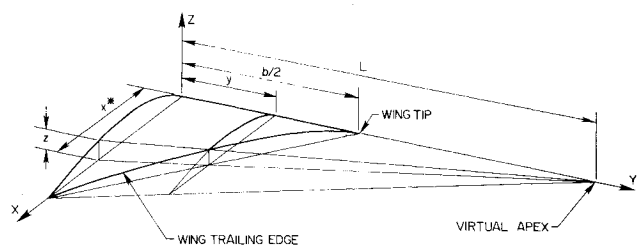

Fig. 2 Wing surface geometry.

Table 1 Model characteristics

Semispan ($b/2$) = 36 in. (91.44 cm)
Wing root width ($c_e + \ell$) = 13.375 in. (33.97 cm)
Wing root chord: adjustable
Planforms
Triangular ($\bar{c} = 1 - \hat{y}$), ℓ = 12 in. (30.48 cm), surface, 0.002 in. (0.05 mm), $\mathcal{R}$ = 9.76
Parabolic ($\bar{c} = \sqrt{1 - \hat{y}}$), ℓ = 12 in. (30.48 cm), surface, 0.004 = in. (0.10 mm), $\mathcal{R}$ = 7.67
Elliptical ($\bar{c} = \sqrt{1 - \hat{y}^2}$), ℓ = 12 in. (30.48 cm), surface, 0.004 in. (0.10 mm), $\mathcal{R}$ = 6.67
Leading-edge streamline shape, c_e = 1.375 in. (3.49 cm), t_e/c_e = 0.409

however, that there is little change in the wing angle of zero lift. Figure 11 shows the effect of excess length on lift-to-drag ratio, indicating the favorable effect of increasing excess length.

Figures 12 and 13 show the effect of Reynolds number (dynamic pressure) on the lift coefficient and lift-to-drag ratio for the parabolic wing. The variations in the lift coefficient near stall and the maximum lift-to-drag ratio indicate that there is a small Reynolds number effect as might be expected in this range. Comparison of Fig. 12 with Fig. 4 showing the effect of apex location indicates that the model was not distorted by variation in dynamic pressure.

Theory

The twist of a wing is normally considered to be composed of two components, the geometric twist due to the rotation of the chord line and the aerodynamic twist due to the variation of the zero-lift angle of the wing section. The development here considers only the wing surface. The presence of the leading-edge spar will, of course, influence the aerodynamic behavior of the model wing. Each of the components of the twist can be described in terms of the membrane shape at the root of the wing since the wing is assumed to be a developable surface. The twist components are expressed in terms of a nondimensional chordwise station $\bar{x}^*$ corresponding to a spanwise station $\hat{y}$. From Fig. 2, defining positive twist as corresponding to an upward movement of the leading edge and assuming a small camber ratio m, the geometric twist is

$$\phi_G = -\bar{z}(\bar{x}^*)/\bar{x}^* \tag{1}$$

The zero-lift line of each section is assumed to be tangent to the three-quarter chord point, and so the aerodynamic twist relative to the zero-lift line at the root of the wing is

$$\phi_A = \frac{d\bar{z}}{d\bar{x}_{.75}} - \frac{d\bar{z}}{d\bar{x}_{.75\bar{x}^*}} \tag{2}$$

The corresponding spanwise location at which these components of twist occur can be seen from Fig. 2 to be

$$\bar{x}^* = \bar{c}(\hat{y}) \Big/ \left(1 - \frac{\hat{y}}{\hat{L}}\right) \tag{3}$$

Now it may be noted that the total twist of the wing surface is due only to the shape of the root section $\bar{z}(\bar{x}^*)$ since, as $\bar{c}(\hat{y}) \to 0$, $\bar{x}^* \to 0$ and, therefore, the twist at the tip of the wing approaches

$$\phi_G \to -\frac{d\bar{z}}{d\bar{x}_{\bar{x}^* \to 0}}$$

$$\phi_A \to \frac{d\bar{z}}{d\bar{x}_{.75}} - \frac{d\bar{z}}{d\bar{x}_{\bar{x}^* \to 0}} \tag{4}$$

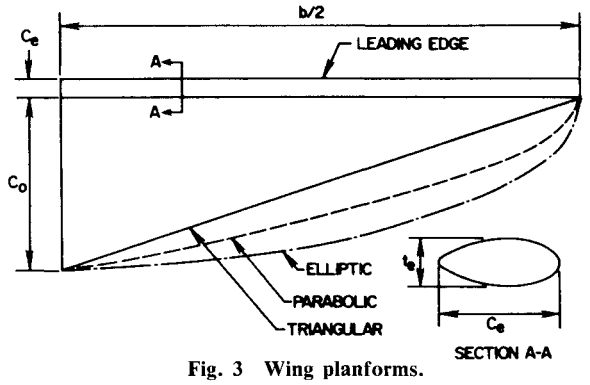

Fig. 3 Wing planforms.

The spanwise twist distribution is determined by Eq. (3) and is thus a function of the wing planform and virtual apex location. It can be shown that for a cambered section that can be represented by a cubic polynomial with the boundary conditions $\bar{z} = 0$ at $\bar{x} = 0$ and $\bar{x} = 1$, the following relationship between the aerodynamic twist and the geometric twist is a good approximation:

$$\phi_A \cong 1.5\phi_G \tag{5}$$

Calculated geometric twist distributions based on Eq. (1) normalized by camber ratio for symmetric camber at the root are illustrated in Figs. 14-16. Figure 14 shows the influence of wing planform on twist distribution for $\hat{L} = \infty$. When the virtual apex is close to the tip of the wing, the triangular wing exhibits a steep twist gradient outboard and, as the apex is moved farther outboard, the twist approaches a linear variation as shown in Fig. 15. With the apex located inboard of the root, the steep gradient occurs inboard. For the parabolic wing as shown in Fig. 16, a similar trend exists although an approximately linear distribution does not occur until the virtual apex is inboard near the root. Figure 17 shows the effect of the location of the maximum camber point on the twist distribution for the parabolic planform. It was not possible during these experiments to determine the shape of the wing section at the root, as in the two-dimensional experiments of Ref. 1 where a small forward shift in maximum camber point with increasing angle of attack was observed.

These analytical results support the experimental trends shown in Figs. 4-10. As the virtual apex location is moved further outboard from the tip, there is an increase in the angle of zero lift or correspondingly a decrease in lift coefficient at a given angle of attack of the wing, and this trend continues as the apex is located inboard of the root. Figures 15 and 16 show that this movement is accompanied by larger negative twist inboard where the chord is larger, thus reducing the lift at a given angle of attack. It was noted in the discussion of the experimental results that varying the excess length (or camber) had little influence on the angle of zero lift. This can be seen to be due to the fact that increasing the camber produces two opposing effects: the first effect reducing the zero-lift angle of attack of the root section, which would increase the lift coefficient at a given angle of attack, is opposed by the increased magnitude of the wing twist, which is proportional to camber (or excess length) as seen from Eqs. (1) and (2).

Figures 18 and 19 provide direct experimental verification of this geometric description of the wing surface by comparing the parabolic and triangular wing lift characteristics with

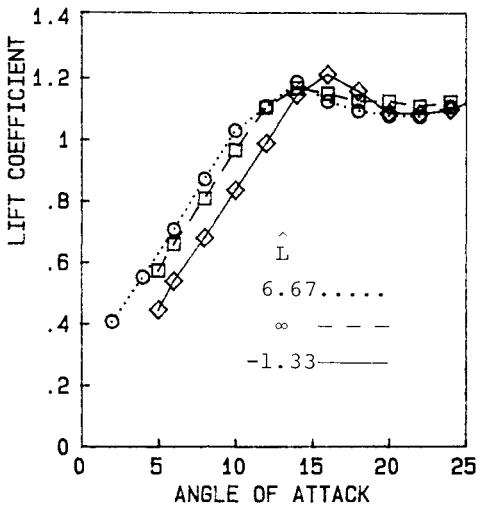

Fig. 4 Lift coefficient vs angle of attack as a function of apex location; parabolic wing, $XL = 0.709$.

the apex location adjusted to give similar twist distributions, as may be seen from Figs. 15 and 16. The spanwise lift coefficient distributions differ on the two planforms at angle of attack, and consequently the different wing planforms exhibit different stall characteristics.

Comparison of Experimental Data with Theory

Given the twist distribution, the planform and camber at the wing root, lifting line theory can be used to estimate the lift characteristics of the wings tested. The twist was calculated based on Eqs. (1) and (2), assuming that maximum camber at the root was at midchord. The simple method of Schrenk[11] was used to estimate the spanwise load distribution and wing lift coefficient. The section properties were based on the experimental results of Ref. 1.

Figures 20 and 21 show very good agreement between theory and experiment below stall.

Maximum section lift coefficients were estimated using the experimental data presented in Ref. 1. Using these data in conjunction with the lift coefficient distribution predicted by Schrenk's method, the maximum wing lift coefficients were estimated and are indicated in Fig. 21 by the filled symbols.

The theoretical approach agrees well with the experimental data confirming the validity of the geometric concepts using

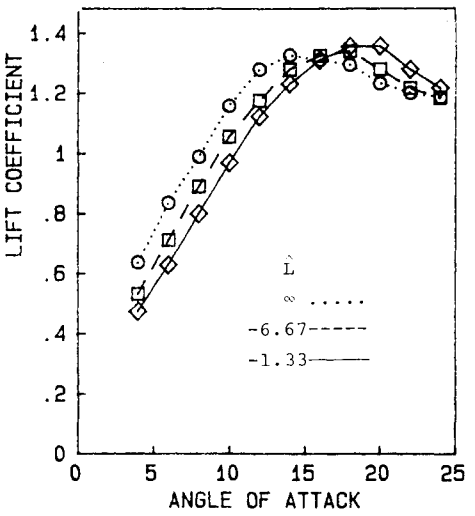

Fig. 5 Lift coefficient vs angle of attack as a function of apex location; parabolic wing, $XL = 1.429$.

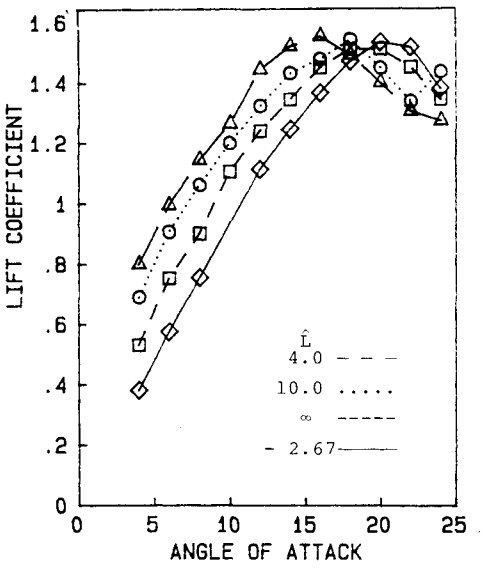

Fig. 6 Lift coefficient vs angle of attack as a function of apex location; parabolic wing, $XL = 2.899$.

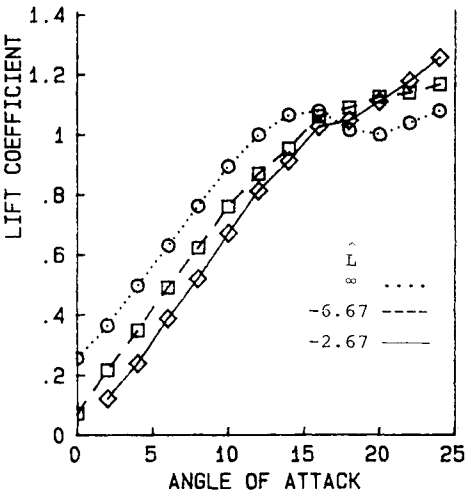

Fig. 7 Lift coefficient vs angle of attack as a function of apex location; triangular wing, $XL = 2.899$.

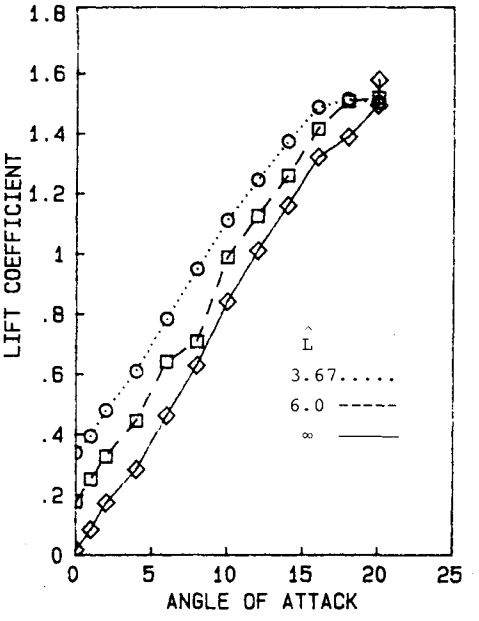

Fig. 8 Lift coefficient vs angle of attack as a function of apex location; elliptical wing, $XL = 0.709$.

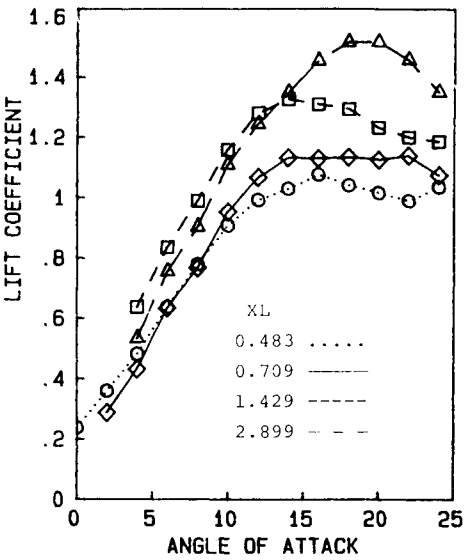

Fig. 9 Lift-to-drag ratio vs angle of attack as a function of apex location; parabolic wing, $XL = 1.429$.

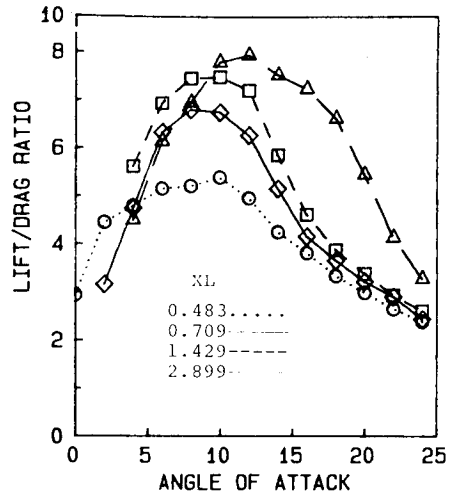

Fig. 10 Lift coefficient vs angle of attack as a function of excess length; parabolic wing, $\hat{L} = \infty$.

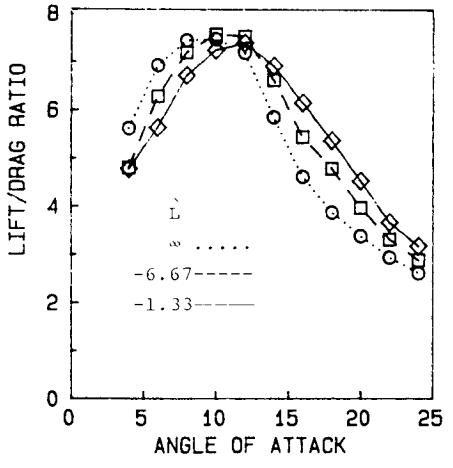

Fig. 11 Lift-to-drag ratio vs angle of attack as a function of excess length; parabolic wing, $\hat{L} = \infty$.

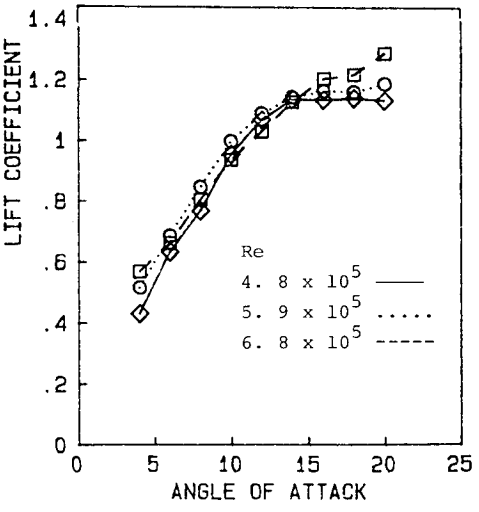

Fig. 12 Effect of Reynolds number on lift coefficient vs angle of attack, $XL = 0.709$, $\hat{L} = \infty$.

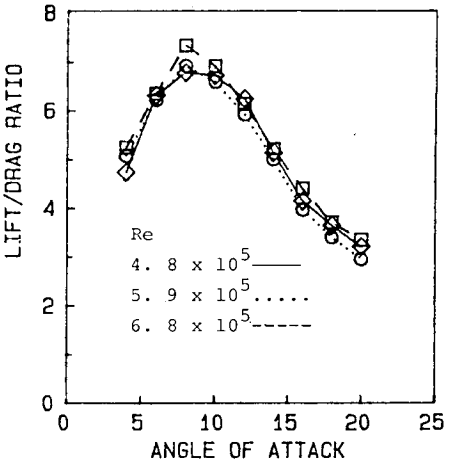

Fig. 13 Effect of Reynolds number on lift-to-drag ratio vs angle of attack; $XL = 0.709$, $\hat{L} = \infty$.

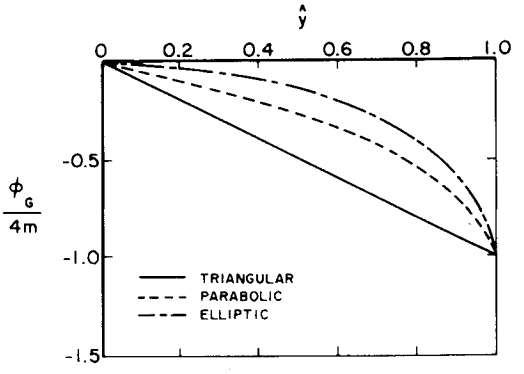

Fig. 14 Geometric twist vs spanwise station for different planforms; symmetric camber, $\hat{L} = \infty$.

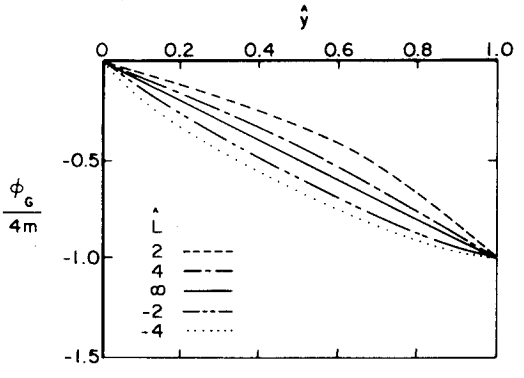

Fig. 15 Geometric twist vs spanwise station as a function of apex location; triangular wing, symmetric camber.

the root section and the virtual apex to define the wing surface geometry.

Unsteady Behavior

Mild oscillatory motions were observed on all planforms in the 15-19 deg angle-of-attack range. The oscillations were of small amplitude and high frequency. This behavior was generally associated with the onset of separation near the root. These limit cycle oscillations would generally occur over a range of 2-3 deg and then disappear as the angle of attack increased further. The 0.002-in. (0.05-mm) parabolic wing also exhibited trailing-edge vibration at moderate angle of attack.

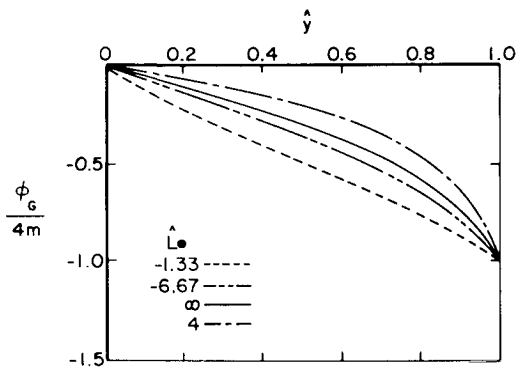

Fig. 16 Geometric twist vs spanwise station as a function of apex location; parabolic wing, symmetric camber.

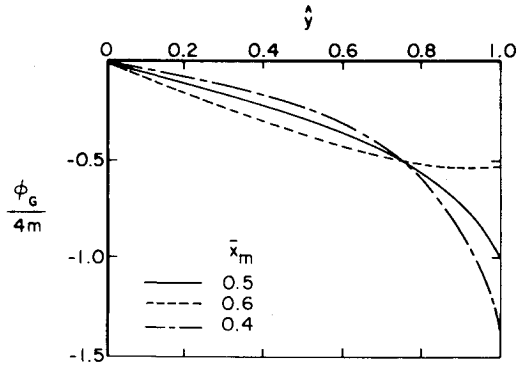

Fig. 17 Effect of camber distribution on geometric twist vs spanwise location; parabolic wing, $\hat{L} = \infty$.

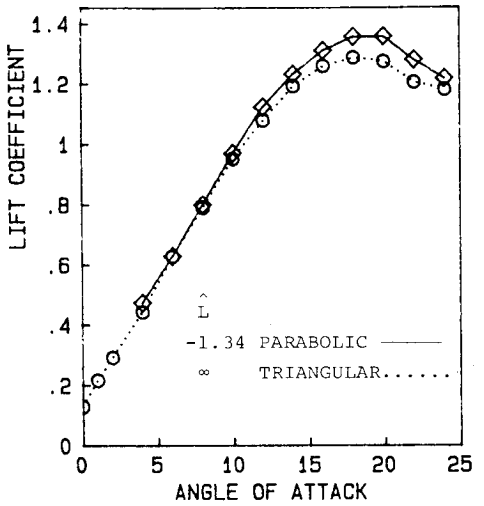

Fig. 18 Comparison of lift characteristics for triangular and parabolic wings with similar twist distributions, $XL = 1.429$.

Unsteady motion was also observed at low angles of attack and was associated with the outer portion of the wing operating at locally negative angles of attack due to wing twist. In general, as the excess length was increased, the angle of attack at which the oscillations commenced increased, indicating dependence on twist. For the small excess length of 0.433%, the lower boundary was about 2 deg whereas, for the large excess length of 2.899%, the boundary increased to 6 deg. The oscillations at the lower limit increased in amplitude and decreased in frequency as the angle of attack was reduced. For the triangular wing, inversion of the wing surface occurred near zero angle of attack for the smallest excess length and at about −2 deg for the larger ex-

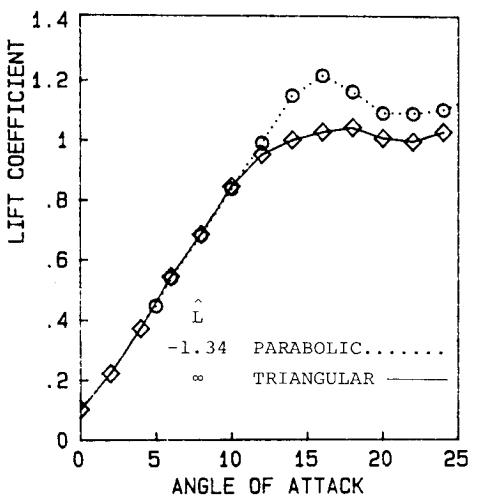

Fig. 19 Comparison of lift characteristics for triangular and parabolic wings with similar twist distributions, $XL = 0.709$.

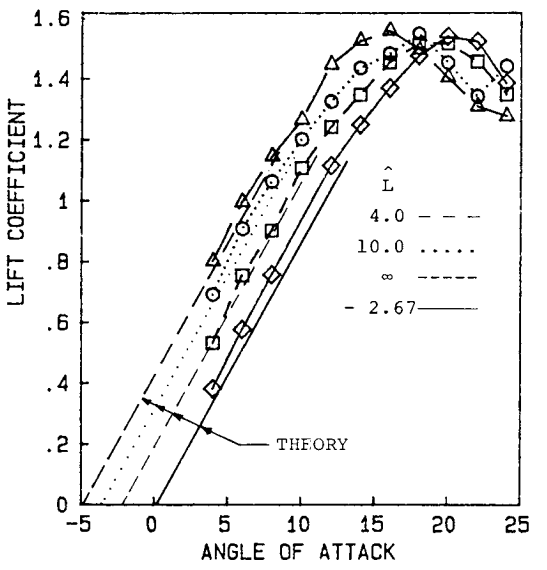

Fig. 20 Comparison of theory and experiment for lift characteristics as a function of apex location; parabolic wing $XL = 2.899$.

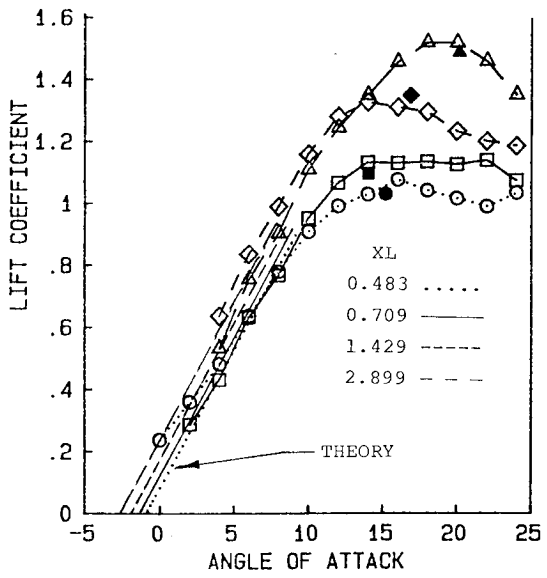

Fig. 21 Comparison of theory and experiment for lift characteristics as a function of excess length; parabolic wing $\hat{L} = \infty$.

cess length. For the parabolic and elliptical wings, inversion damaged the wing surface at dynamic pressures above 4 psf, and so the lower angle-of-attack ranges were not investigated.

Conclusions

1) The geometrical concept of using the root section together with the virtual apex to define the wing geometry was validated by comparison of experiment and theory for the ranges covered in the experiment. This concept simplifies the description of the wing shape.

2) The operating range of the membrane wings tested is limited by stall and separation at high angles of attack and by oscillatory behavior at low angles of attack. The operating range is also influenced by wing shape, excess length, virtual apex position, and dynamic pressure.

3) Within the range of variables studied, the angle of attack at which separation occurs increases with increasing excess length and also increases with apex position due to the change in twist distribution. It is also influenced by the planform shape.

4) For all the wings tested, a benign stall characteristic was observed.

5) A parabolic planform membrane wing of very thin stainless steel can support a pressure differential across the sheet without the aid of a trailing-edge support member. This was true for the elliptical planform only at very low dynamic pressures.

References

[1]Greenhalgh, S., Curtiss, H. C. Jr., and Smith, B., "Aerodynamic Properties of a Two-Dimensional Inextensible Flexible Airfoil," *AIAA Journal*, Vol. 22, July 1984, pp. 865-870.

[2]Thwaites, B., "The Aerodynamic Theory of Sails, I. Two-Dimensional Sails," *Proceedings of the Royal Society of London*, Vol. 261, 1961, pp. 402-422.

[3]Nielsen, J. N., "Theory of Flexible Aerodynamic Surfaces," *Journal of Applied Mechanics*, Vol. 30, 1963, pp. 435-442.

[4]Curry, M., *Yacht Racing—The Aerodynamics of Sails and Racing Tactics*, Henry Holt and Co., New York, 1927, pp. 69-83.

[5]Tanner, T., *A Review of Three-Dimensional Sail Aerodynamics*, University of Southampton, U.K., Dec. 1969.

[6]Marchaj, C. A., *Aero-Hydrodynamics of Sailing*, Dodd-Mead, New York, 1979, pp. 548-653.

[7]Milgram, J. H., "The Analytical Design of Yacht Sails," presented at the Annual Meeting of the Society of Naval Architects and Marine Engineers, New York, NY, Nov. 1968.

[8]Jackson, P., "A 3-D Aeroelastic Sail Model," *Proceedings of Conference on the Science of Sail Design Characteristics*, University of Western Ontario, London, Canada, June 1982.

[9]Ormiston, R. A., "Theoretical and Experimental Aerodynamic of an Elastic Sailwing," Ph.D. Dissertation, Department of Aerospace and Mechanical Sciences, Princeton University, Princeton, NJ, Oct. 1969.

[10]Kroo, I., "Aerodynamics, Aeroelasticity, Stability of Hang Gliders," Ph.D. Dissertation, Department of Aeronautics and Astronautics, Stanford University, Stanford, CA, 1983.

[11]Schrenk, O., "A Simple Approximation Method for Obtaining the Spanwise Lift Distribution," NACA TM 948, 1940.

[12]Greenhalgh, S., "A Three Dimensional Inextensible Lifting Membrane Wing—Experimental Results," Naval Air Development Center, Warminster, PA, Rept. 83130-60, Oct. 1983.